Photoconductivity of PbSe Quantum-Dot Solids: Dependence on Ligand Anchor Group and Length

Yunan Gao,[†,‡] Michiel Aerts,[†] C. S. Suchand Sandeep,[†] Elise Talgorn,[†] Tom J. Savenije,[†] Sachin Kinge,[§] Laurens D. A. Siebbeles,[†,*] and Arjan J. Houtepen[†,*]

[†]Optoelectronic Material Section, Department of Chemical Engineering, Delft University of Technology, Julianalaan 136, 2628 BL, Delft, The Netherlands, [‡]The Kavli Institute of Nanoscience, Delft University of Technology, Lorentzweg 1, 2628 CJ, Delft, The Netherlands, and [§]Materials Research & Development, Toyota Motor Europe, Hoge Wei 33, B-1930 Zaventem, Belgium

ABSTRACT The assembly of quantum dots is an essential step toward many of their potential applications. To form conductive solids from colloidal quantum dots, ligand exchange is required. Here we study the influence of ligand replacement on the photoconductivity of PbSe quantum-dot solids, using the time-resolved microwave conductivity technique. Bifunctional replacing ligands with amine, thiol, or carboxylic acid anchor groups of various lengths are used to assemble quantum solids *via* a layer-by-layer dip-coating method. We find that when the ligand lengths are the same, the charge carrier mobility is higher in quantum-dot solids with amine ligands, while in quantum-dot solids with thiol ligands the charge carrier lifetime is longer. If the anchor group is the same, the charge carrier mobility is ligand length dependent. The results show that the diffusion length of charge carriers can reach several hundred nanometers.

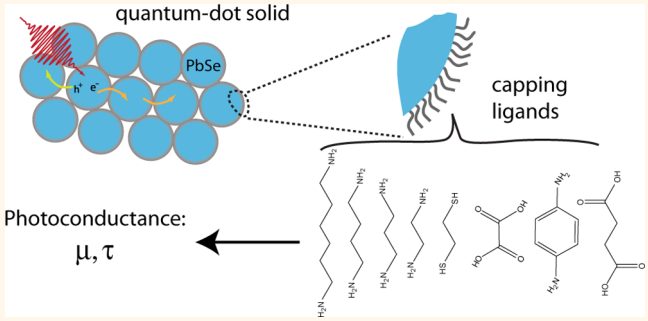

KEYWORDS: quantum dots · solar cells · carrier mobility · carrier lifetime · photoconductivity. layer-by-layer assembly

Recently the research on thin films of quantum dots (QD), so-called QD solids, has achieved great progress toward many applications, such as photodetectors,[1] field-effect transistors,[2−4] and solar cells.[5−11] These applications require conductive QD solids, in which QDs are electronically coupled and charge carriers can efficiently move to electrodes. By wet synthesis techniques[12−14] narrow size distribution, low-cost QDs have been made successfully, but these QDs have long and insulating native capping ligands that should be replaced by short ligands to get a conductive film. The replacing ligands significantly influence the properties of a QD solid and determine to a large extent the performance of QD devices.

Much progress has been made by introducing smaller organic ligands,[15] metal chalcogenide ligands,[2,16] thiocyanate ligands,[17] or metal-free inorganic ligands.[18,19] Ligand exchange is often done after film formation. This is achieved by drop casting or spin coating followed by soaking in a solution of replacing ligands or by layer-by-layer (LbL) dip coating with ligand exchange during each cycle of the LbL process. The dip-coating technique has been shown to be successful in fabricating high-quality QD solids, which are homogeneous and crack free and show high charge carrier mobilities.[20,21]

Various organic molecules with different anchor groups, such as amine,[3,20,22−25] thiol,[10,20,21,26−32] or carboxylic acid,[33] and with different lengths have been used as replacing ligands. Carrier mobilities of ~1 $cm^2/(V\ s)$ are reported for drop-casted QD solids treated with hydrazine,[3] while in refs 28 and 33 10-fold lower mobilities are measured for LbL dip-coated solids treated with 1,2-ethanedithiol or formic acid. Several studies have appeared reporting different replacing ligands; however a systematic comparison is lacking. A variety of preparation methods have been used to fabricate QD solids, and the charge carrier mobilities were determined by different methods. Moreover, in contrast to the large number

* Address correspondence to a.j.houtepen@tudelft.nl; l.d.a.siebbeles@tudelft.nl.

Received for review July 3, 2012 and accepted October 18, 2012.

Published online October 18, 2012
10.1021/nn3029716

of studies on charge carrier mobility, only a few studies on carrier kinetics exist.[23]

Here we present a systematic study on the influence of the replacing ligands on charge carrier mobility and carrier lifetime in PbSe QD solids, using the time-resolved microwave conductivity technique (TRMC). TRMC determines the local ac photoconductivity. The conductivity is probed in a film domain with a typical size of ~30 nm. Therefore TRMC measures the intrinsic charge transport properties and is not sensitive to global film properties such as cracks. We focus on small organic replacing ligands, as these have been, so far, the most used in the fabrication of QD solar cells and photodetectors. The QD solids are fabricated using the LbL dip-coating method and are homogeneous and crack-free, as shown by scanning electron microscopy (SEM) images (see Supporting Information). The replacing ligands 1,2-ethanediamine (EDA), 1,2-ethanedithiol (EDT), and oxalic acid (OxAc) are used to investigate the influence of the anchor group on the photoconductivity, while a series of alkyldiamines of variable length, 1,4-benzenediamine (BeDA) and butanedioic acid (BuAc), are used to study the influence of ligand length. We find that with amine as an anchor group the charge carrier mobility is almost 1 order of magnitude higher than with thiol or acid anchor groups, when ligands have comparable lengths.

The effect of increasing the ligand length is, as expected, a reduction of the carrier mobility due to the increase in the width of the tunnel barrier between QDs. This shows that the replacing ligands do indeed determine the interparticle spacing. Among the ligands studied here, we find the highest mobility of 2 $cm^2/(V\ s)$ in QD solids with EDA ligands, while the longest carrier lifetime of 18.5 ns is found using EDT.

RESULTS AND DISCUSSION

PbSe QDs with oleylamine capping ligands are synthesized following ref 13. QD solids are prepared with the layer-by-layer dip-coating method using a Nima DC multi-8 dip coater installed in a nitrogen glovebox. Because oleylamine is a weaker binding ligand than the more "traditional" oleic acid capping ligand, we expect a faster and more efficient ligand exchange. Indeed, Fourier transform infrared (FTIR) spectra show a great reduction of the absorption in the CH_2-stretch vibration region upon ligand exchange (see Figure S1 in the Supporting Information). Figure 1a and b show optical absorptance spectra (the fraction of absorbed light *vs* wavelength) of QD solids and their QD mother dispersions in tetrachloroethylene (TCE). The optical absorptance spectra of the QD solids show a red-shift and broadening compared with the spectra of QDs in dispersion. This is a common observation that has been discussed elsewhere.[34−36] Note that for EDT the red-shift is much more pronounced than for the other ligands. This is visible both in Figure 1a, where 3.9 nm

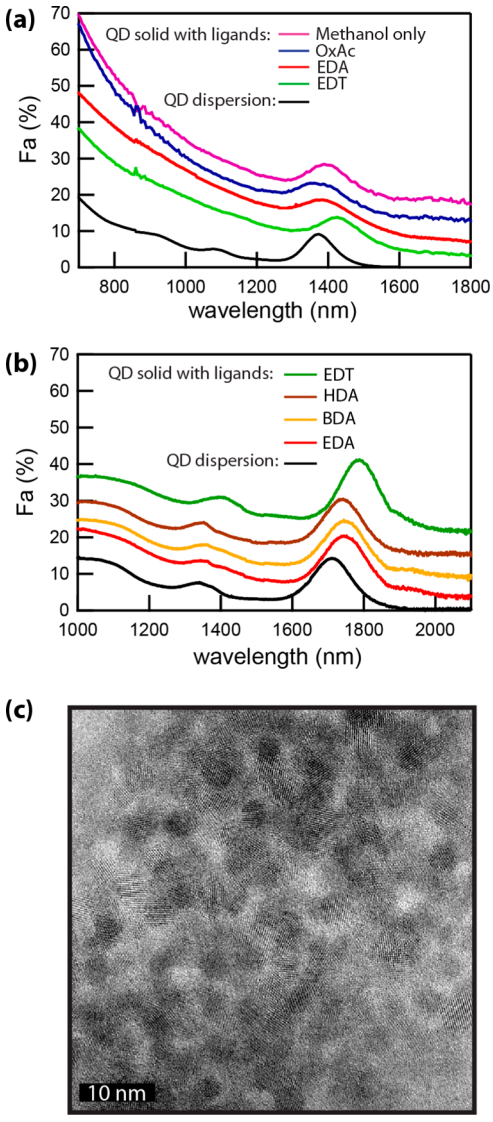

Figure 1. (a) Absorptance spectra of 3.9 nm PbSe QD solids prepared using the layer-by-layer dip-coating method on quartz substrates with various replacing ligands: EDA (red line), EDT (green line), OxAC (blue line) and without ligands (rinsed with pure methanol, magenta line). The spectra are offset for clarity. (b) Absorptance spectra of 6.0 nm PbSe QD solids with a series of alkydiamine ligands: EDA (red line), BDA (orange line), HDA (brown line), and EDT (green line). (c) High-resolution TEM image of a PbSe EDA QD film prepared by a single dip-coating cycle.

diameter PbSe QD solids are compared, and in Figure 1b, which shows 6.0 nm diameter PbSe QD. A similar observation is made for long dodecyl thiol ligands, while no red-shift is observed upon exchange to dodecylamine (see Supporting Information, Figure S2). This shows that part of the large red-shift observed with EDT is not caused by electronic coupling between QDs but is due to interaction of the thiol group with the QDs, in line with an earlier observation of Liu *et al.*[28]

Figure 1c shows a high-resolution TEM image of a submonolayer of PbSe QDs treated with EDA and demonstrates that the QDs do not merge into big particles or wires. However, given the very small expected

length of the shortest ligands (~0.4 nm for 1,2-ethanediamine), the TEM images do not allow us to rule out a small amount of necking between particles. We note that the substrate for the TEM measurement shown in Figure 1b is silicon nitride, while TRMC measurements are performed on silanized quartz substrates. Furthermore, the imaged sample is made with only a single dip-coating cycle. Hence the TEM image may not fully represent the organization of QDs in the thicker solids. It is concluded from the TEM image and the absorptance spectra that the QDs do not merge significantly during the LbL assembly and still contain features of quantum confinement.

The room-temperature photoconductivity of these QD solids is measured using the TRMC technique.[20,37−39] Details on this technique can be found in the Methods section. The sample is excited with a tunable nanosecond laser pulse, resulting in the generation of charge carriers. The accompanying increase in conductivity is determined by measuring the increase of the absorption of microwave radiation. As shown in the inset of Figure 2a, charge generation during the laser pulse results in an increase of the measured conductivity, followed by a decrease as charges relax or recombine. Figure 2a shows the maximum value of the photoconductance transients, $\phi_{max}\Sigma\mu$, as a function of the average number of photons absorbed per QD, $\langle N_{abs}\rangle$, which is calculated as $\langle N_{abs}\rangle = I_0\sigma$, where I_0 is the photon fluence in the laser pulse and σ is the absorption cross section taken from ref 40. In the product $\phi_{max}\Sigma\mu$, ϕ_{max} is the maximum measured yield of mobile charge carriers per absorbed photon and $\Sigma\mu$ is the sum of the electron and hole mobility. As shown in the figure, $\phi_{max}\Sigma\mu$ increases as the photoexcitation density decreases; in the low excitation regime (below 0.001 absorbed photon per QD) the value of $\phi_{max}\Sigma\mu$ is virtually independent of $\langle N_{abs}\rangle$. The lower values of $\phi_{max}\Sigma\mu$ at higher $\langle N_{abs}\rangle$ are attributed to Auger recombination, which at high excitation density decreases the number of mobile charges during the laser pulse duration and the response time of the setup.[41] At low intensity, higher order recombination can be ignored. In this case the photon to carrier yield, ϕ_{max}, is close to the quantum yield, η, of charge carrier photogeneration. Recently we have shown that η is close to 1 in EDA-treated PbSe QD solids;[41] hence the value of $\phi_{max}\Sigma\mu$ at low intensity is equal to the sum of the electron and hole mobilities, at least for EDA-treated PbSe QD solids.

From Figure 2a the following observations can be made: (1) Even without any replacing ligands (only rinsing the film with methanol, which is the solvent for all replacing ligands), conductive QD solids are prepared with carrier mobilities similar to those obtained with EDT and OxAc ligands. (2) For EDA ligands the mobilities we determine are as high as 2 $cm^2/(V\ s)$, which is higher than mobilities reported in the literature for similar systems.[3,28] (3) In Figure 2a the EDA-treated QD solid has a carrier mobility that is 7 times

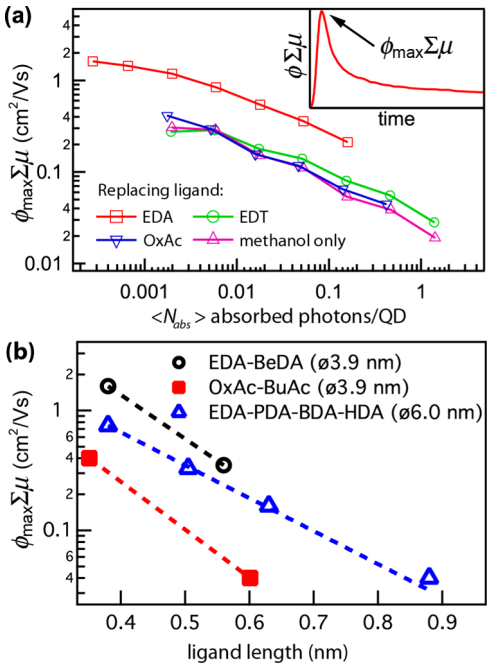

Figure 2. TRMC photoconductivity of PbSe QD solids with different replacing ligands, as indicated in the figure. (a) $\phi_{max}\Sigma\mu$ values as a function of the average photoexcitation density for QD solids with different replacing ligands. The inset shows a photoconductivity transient and the corresponding value of $\phi_{max}\Sigma\mu$. (b) Overview of the effect of ligand length on the $\phi_{max}\Sigma\mu$ values for various series of ligands: 1,2-ethanediamine and 1,4-benzenediamine (black circles), oxalic acid and butanedioic acid (red squares), and 1,2-ethanediamine, 1,3-propanediamine, 1,4-butanediamine, and 1,6-hexanediamine (blue triangles). The dashed lines are exponential fits to the data.

higher than the EDT/OxAc-treated QD solids, while the length of these ligands is comparable. The exact difference in mobility between EDA- and EDT/OxAc-treated films varies between 5 and 30 over all the samples we have investigated and is typically an order of magnitude. We note that the similarity in $\phi_{max}\Sigma\mu$ between EDT-, OxAc-, and MeOH-treated films in Figure 2a is probably coincidental.

The first feature suggests that the solvent, which is used to carry the replacing ligands, plays a very important role in the assembly of conductive QD solids. We note that the photoconductivity of drop-casted QD films, where the original oleylamine is still present, is below the detection limit of our TRMC setup. This implies that $\phi_{max}\Sigma\mu < 10^{-4}$ $cm^2/(V\ s)$ with the original ligands in place. Therefore, it appears that methanol is able to remove the oleylamine ligands. This is in line with a previous report that shows that ethanol partially removes oleate ligands from the surface of PbSe QDs, forming ethoxide at the particle surface.[22] This process is triggered by protonation of surface-bound oleate by the weakly acidic ethanol. A significant difference from the above-mentioned study is that in the present measurements the native ligands were oleylamine. Oleylamine is known to bind much more weakly to

the PbSe surface than oleate.[13] Most likely the oleylamine ligands are in a fast dynamic exchange with free oleylamine in solution, as is the case for primary amines on CdTe[42] and PbS[14] QDs. Thus, exposing the oleylamine-capped particles to solvents in which oleylamine can partially dissolve will result in a decrease of ligand density. The resulting empty surface sites may be (partially) passivated with methanol or methoxide.

We have observed that using acetonitrile instead of methanol has a similar effect: films can be deposited without addition of a deliberate replacing ligand; the photoconductivity in the acetonitrile-grown films is comparable (see Supporting Information, Figure S4). Earlier studies showed little effect of acetonitrile. For instance, using small-angle X-ray scattering, Law *et al.* observed no effect on the interparticle separation when exposing PbSe QD films to acetonitrile, while a clear reduction of the interparticle spacing was observed upon exposure to pure ethanol.[22] We speculate that the weaker binding to the PbSe surface of oleylamine compared to oleate[13] allows for ligand removal even in the absence of acidic solvents. Acetonitrile itself has a significant affinity for gold surfaces, with a binding energy of ~50 kJ/mol (0.5 eV/molecule).[43,44] While the interaction between acetonitrile and the PbSe surface is, to the best of our knowledge, not known, it seems likely that the oleylamine ligands are replaced with weakly bound acetonitrile molecules. When ligands are added (either in methanol or in acetonitrile) that have a stronger affinity for the surface than the solvent molecules, these ligands will (at least partially) bind to the particle surface.[21,22]

The second observation that can be made from Figure 2a is that the carrier mobility we determine for PbSe QD solids with EDA ligands is as high as 2 $cm^2/(V\,s)$. This mobility is higher than the mobility reported in ref 3 for hydrazine-treated films, while hydrazine is an even shorter ligand than EDA. This difference could partially result from the layer-by-layer dip-coating method employed here, during which the ligand exchange has been shown to be more complete.[20] Another reason for the higher mobility reported here is that different techniques (TRMC here *vs* field-effect transistors (FETs) in refs 3, 28, and 33) were used to determine the carrier mobility. TRMC determines ac carrier mobilities and probe charge transport on a local scale. We use 8.4 GHz microwave radiation as a probe. In half a period of this microwave field, the carrier diffusion length is ~42 nm, estimated using the Einstein–Smoluchowski equation $LD = (6k_BT\mu/(2fe))^{1/2}$, where k_B is the Boltzmann constant, T is room temperature, μ is the carrier mobility of 2 $cm^2/(V\,s)$, e is the elementary charge, and f is the frequency of the microwave probe field. In FET measurements, the channel width is several micrometers. If there is variation in electronic coupling on a length scale between 42 nm and 1 μm, the carrier mobility will be lower in FET measurements than in TRMC measurements.[34] The carrier mobility difference with FET measurements is also observed for the QD solids with other replacing ligands. For EDT, we get a 20 times higher carrier mobility than reported in ref 28, and for OxAc a similar ratio holds with respect to ref 33.

Our third observation from Figure 2a is that EDA QD solids have a 10-fold higher carrier mobility than QD solids prepared with EDT, with oxalic acid, or without intentional replacing ligands (*i.e.*, rinsing with methanol or acetonitrile only). Several reasons are considered. With the amine group the ligand replacement could be more complete. However this is not in line with many existing reports that show that the ligand exchange is very efficient with 1,2-dithiol in alcohols.[22] In addition, FTIR spectra of EDT-treated films show an almost complete removal of the absorption features related to CH_2 vibration, suggesting efficient removal of the original ligands (Supporting Information, Figure S1).

Another possible explanation could be that the amine ligands might result in a lower tunnel barrier. Although the HOMO–LUMO gaps and the electron affinities of alkyldiamines, alkyldithiols, and alkyldicarboxylic acids are not expected to be very different,[45] significant differences have been observed in the electronic conductance of single molecules of these species.[46–48] Tao *et al.* have investigated the single-molecule conductance of alkyldithiols, -diamines, and -dicarboxylic acids for various lengths of the alkyl chain.[47] Their results are well described by the tunneling expression:

$$G = A \exp(-\beta d) \quad (1)$$

where G is the single-molecule conductance, A is a constant determined by the molecule–electrode coupling strength, β is the tunneling decay constant, and d is the length of the alkyl chain. For the various anchor groups they studied they found comparable values of β (0.87 $Å^{-1}$ for dithiols, 0.70 $Å^{-1}$ for diamines, and 0.57 $Å^{-1}$ for dicarboxylic acids). A much larger variation was observed in the constant A for the various anchor groups, with $A_{thiol} \gg A_{amine} \gg A_{carboxylic\ acid}$. This variation was attributed to a difference in electronic coupling between the anchor groups and the gold electrodes used in the single-molecule conductance experiments.

The electronic coupling between PbSe QDs and the various anchor groups could be different from the coupling between the anchor groups and gold. However, to the best of our knowledge, very little is known about the electronic coupling between PbSe QDs and ligand anchor groups. Therefore it is unclear whether differences in electronic coupling between the anchor groups and the PbSe QD surface give rise to differences in the measured charge carrier mobility. We note that strong electronic coupling between the ligands and

conduction or valence electron levels could result in a shift of the optical transition energies. A clear red-shift is, for instance, observed for CdTe QDs upon exchanging amine for thiol ligands and has been attributed to an effective delocalization of the electron and hole wave function over the thiol anchor group.[49] A similar red-shift is observed here for exchange of the original ligands for dodecylthiol (see Supporting Information, Figure S2). This suggests strong coupling between the thiol group and the electronic levels in the QDs, which, however, apparently does not result in high charge carrier mobilities. We must conclude that the reason for the significantly higher photoconductivity of amine-based ligands remains unclear.

Besides the anchor group, the ligand length also affects the carrier mobility. Figure 2b shows the carrier mobility length dependence of various ligands. The blue triangles represent the 6.0 nm PbSe QD samples shown in Figure 1b, where the ligands consist of alkyldiamine molecules of variable chain length: 1,2-ethanediamine (EDA), 1,3-propanediamine (PDA), 1,4-butanediamine (BDA), and 1,6-hexanediamine (HDA). Also shown in Figure 2b are the mobilities for 3.9 nm PbSe QD solids with EDA and 1,4-benzenediamine ligands and OxAc (black circles) and BuAc ligands (red squares). The lengths shown on the *x*-axis of Figure 2b are the lengths of the ligands as estimated from the molecular geometries optimized using the semiempirical method AM1 in Spartan '02. EDA has an estimated length of 0.38 nm, 1,4-benzenediamine has a length of 0.56 nm, oxalic acid is 0.35 nm, and 1,4-butanedioic acid is 0.61 nm. For the longer alkyldiamines a nominal length of 0.125 nm of each C−C bond is assumed.[28]

A study of carrier mobility ligand length dependence with alkyldithiol replacing ligands has been reported in ref 28. At room temperature, the carrier transport in these QD solids is usually described by the Miller−Abrahams hopping rate,[50,51] and the mobility depends exponentially on interparticle distance,[57] analogous to eq 1. From the mobility at low excitation density, as shown in Figure 2b and the lengths of the ligands used, we determine a value of 0.63 $Å^{-1}$ for the alkyldiamine ligands (blue triangles), a value of 0.9 $Å^{-1}$ for EDA *vs* BeDA (black circles), and a value of 0.8 $Å^{-1}$ for the carboxylic acid ligands (red squares). These values agree reasonably well with the value of 1.0 $Å^{-1}$ for PbSe QD solids with alkyldithiol ligands[52] reported in ref 28 and are in general consistent with tunneling decay parameters for saturated single molecules or self-assembled monolayers.[53] Surprisingly we find that the distance dependence for EDA−BeDA, which involves the aromatic BeDA ligands, is stronger than the distance dependence of the linear alkyldiamines, while the opposite is expected from single-molecule conductance experiments. The reason for this observation is not clear. It is conceivable that the interparticle distance is smaller than the estimated ligand length in the case of linear alkyldiamines, as these molecules are flexible and could even bind in a bidentate fashion to a single nanocrystal. This is not expected for 1,4-benzenediamine, as this is a rigid molecule. Even if this is the case, the observed β value of 0.9 $Å^{-1}$ for EDA−BeDA is high and more commonly observed for linear alkyl chains than for aromatic molecules. It appears that there is little benefit of using this aromatic molecule over saturated replacing ligands of similar length. Our results show that the ligand length dependence of the mobility is a general phenomenon if the same anchor group is used.

In addition to the carrier mobility, the carrier lifetime is another key factor that influences device performance. Figure 3a shows normalized decay traces for a PbSe QD solid with EDA replacing ligands at various photoexcitation densities. At high photoexcitation density the decay of the photoconductivity becomes slower with decreasing intensity. At low excitation density however the decay becomes independent of intensity and the transients overlap. The inset in Figure 3a shows the difference between the normalized photoconductivity transients at 0.018 and 0.006 absorbed photon per QD. This difference is clearly within the noise of the measurement. This implies that higher order decay processes (Auger recombination, Langevin recombination) do not play a significant role and that the remaining decay is a first-order process. Note that the decay times are much shorter than the radiative lifetime, which is on the order of 1 μs for PbSe QDs.[54] This is in line with the absence of detectable photoluminescence in these films. Most probably the observed first-order decay is due to surface trap induced nonradiative decay. During the assembling process a large fraction of the native ligands are removed, and the passivation with replacing ligands could be incomplete, leaving dangling bonds at the surface. These dangling bonds could act as sites for charge carrier trapping. However there could also be other kinds of traps. For instance, domains could exist where several nanoparticles have sintered together, resulting in low-energy sites within the film.

We have previously shown (Supporting Information of ref 41) that the decay of charge carriers is thermally activated. This is shown again in Figure 3b, which presents photoconductivity transients at temperatures between 90 and 300 K. It is clear that the first-order decay of the photoconductivity is strongly temperature activated. This is summarized in the inset in Figure 3b, which shows the half-lifetime $\tau_{1/2}$ at low excitation density ($\langle N_{abs} \rangle$ = 0.001) as a function of temperature. While the temperature activation does not unveil the chemical nature of the trapping sites, it is in line with thermally activated charge trapping at surface sites. The density and the nature of such traps could depend on the replacing ligands that are used in

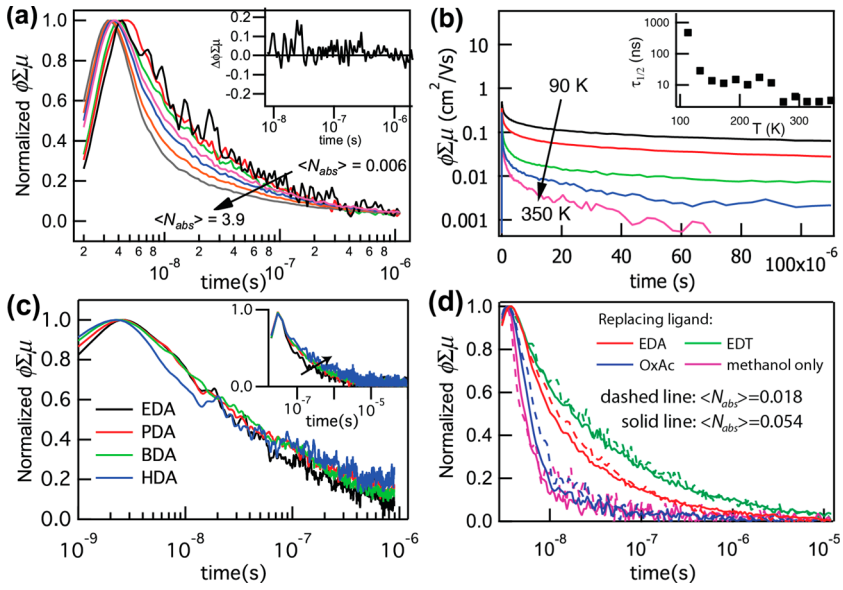

Figure 3. (a) Normalized photoconductivity transients for a PbSe QD solid with EDA replacing ligands at various excitation densities: 0.006 (black), 0.018 (red), 0.054 (green), 0.15 (purple), 0.45 (blue), 1.3 (orange), and 3.9 (gray) absorbed photons per QD. The inset shows the difference between the two transients at the lowest fluences, demonstrating that within the noise of the experiments these transients are the same. (b) Temperature-dependent photoconductivity transients for PbSe QD solids with EDA ligands. The inset shows the extracted half-lifetime at low excitation density ($\langle N_{abs} \rangle$ = 0.001) as a function of temperature. (c, d) Normalized photoconductivity for PbSe QD solids with ligands of various length (c) or various anchor groups (d). The inset in (c) shows the transients on a longer time scale. The solid and dashed lines in (d) correspond to $\langle N_{abs} \rangle$ = 0.054 and $\langle N_{abs} \rangle$ = 0.018 absorbed photon per QD, respectively.

the film preparation procedure, resulting in decay kinetics and charge carrier lifetimes that vary with ligand type.

Figure 3c compares the decay kinetics of the QD solids with alkyldiamine ligands of various chain lengths. Chemically these samples are very similar, as the QD surfaces are passivated with amine groups. However, they differ strongly in the mobility of the charge carriers, as shown in Figure 2b. We find that on a ~100 ns time scale the decay kinetics of the various alkyldiamine-treated samples are very similar. Apparent differences are within the noise level of the measurements (especially important for the low-mobility HDA-treated film). On a longer time scale (inset of Figure 3c) the photoconductivity decay becomes slower as the mobility of the samples decreases (from EDA to HDA). The fact that the initial decay is insensitive to the charge carrier mobility suggests that diffusion of charges does not play a role. This is in line with the presence of abundant trap sites at the QD surface, resulting in a reaction-limited trapping rate. On a longer time scale the decay of the photoconductivity could be attributed to trap-mediated electron−hole recombination involving diffusion of charge carriers that are thermally excited out of the traps. Alternatively the observed decay kinetics can be explained by fast trapping of the most mobile charge carrier (presumably the electron[28]) on abundant surface traps, followed by diffusion-mediated recombination with the less mobile charge carrier on longer time scales.

In contrast to the subtle changes in decay kinetics for the various alkyldiamine-treated samples, Figure 3d shows clear differences in the decay kinetics of QD solids treated with ligands that contain different anchor groups. The carrier half-lifetime ($\tau_{1/2}$) in the QD solid with EDT ligands is 18.5 ns, while the carrier lifetime with EDA ligands is 12.5 ns. With oxalic acid, or when preparing the QD films with methanol only, the obtained half-lifetimes are ~5 ns and are most likely limited by the instrumental time resolution. We note that the observed half-lifetimes are sensitive to the exact film preparation conditions; however the trend in lifetimes with varying replacing ligand is reproducible. Hence, while EDT ligands result in a significantly lower peak photoconductivity, the charge carrier lifetime is significantly longer than for the other ligands, including EDA. These variations could reflect a variation in the degree of surface passivation. EDT is expected to bind the strongest to the surface and could have the highest degree of passivation.

TABLE 1. Summary of Charge Carrier Properties in PbSe QD Solids with Various Replacing Ligands at Room Temperature

replacing ligands	$\Phi_{max}\Sigma\mu$ (cm²/(V s))	$\tau_{1/2}$ (ns)	diffusion length (nm)
EDA	1.6	12.5	550
EDT	0.27	18.5	280
OxAcid	0.41	<5.0	
methanol only	0.30	<7.5	

For the performance of diffusion-driven solar cells, the carrier diffusion length, $L_D = (6\tau_{1/2}k_BT\mu/e)^{1/2}$, determines how efficiently the carriers can be harvested.

Table 1 summarizes the carrier mobility, lifetime, and diffusion length for short-ligand solids at room temperature. QD solids with EDA ligands demonstrate a diffusion length of 550 nm, which should be sufficient to extract charges from a QD solar cell with a thickness of the QD absorber layer of several hundred nanometers. On the basis of the results in Table 1 the use of EDA in QD solar cells would be preferred over the much more commonly used EDT. However the diffusion length is only one of the aspects that determine the solar cell efficiency. In addition, the diffusion lengths presented in Table 1 are derived from the total photoconductivity, which is due to electrons and holes. If one of these two carriers has a significantly shorter diffusion length than the other, it could form a bottleneck for the solar cell efficiency. In practice it has proved difficult to construct efficient solar cells using EDA ligands,[55] while many solar cells employing dithiols are reported.[56,57]

CONCLUSION

In conclusion, the effects of replacing ligands on photoconductivity of PbSe QD solids were systematically studied, and several conclusions are drawn. (1) The solvent, methanol or acetonitrile, used for the chemical treatment can sufficiently remove and replace the native oleylamine ligands and therefore plays an important role in fabricating conductive QD solids. (2) The anchor group of replacing ligands strongly affects the carrier mobility and lifetime. With amine anchor groups the QD solids show higher carrier mobilities, while with thiol groups the QD solids possess a longer carrier lifetime. The carrier lifetime at low excitation density is determined by trapping processes on a nano- to microsecond time scale. (3) For all anchor groups investigated in this paper, the carrier mobility decreases exponentially with ligand length.

METHODS

Quantum Dot Synthesis. We used an oleylamine-based synthesis[13] that results in weakly bound ligands that are easily replaced. A 14 mL amount of oleylamine and 0.38 g of $PbCl_2$ were degassed under vacuum at 100 °C, followed by heating to 140 °C under nitrogen. A 260 μL sample of $Sn[N(SiMe_3)_2]_2$ dissolved in 2 mL of trioctylphosphine (TOP) and 6 mL of 1 M Se in TOP solution were prepared in two vials in a glovebox. Then these two precursors were mixed in a syringe and immediately injected into a $PbCl_2$/OLA solution. The QDs were allowed to grow to the desired size at 112 °C, and the reaction mixture was cooled with a water bath. The resulting solution was filtered with a 200 nm pore size filter to remove residual $PbCl_2$. Then the QDs were precipitated with butanol, centrifuged at 5000 rpm for 10 min, and finally dried under vacuum. The QDs were dispersed in tetrachloroethylene for optical measurements and in hexane for dip-coating. Particle diameters were determined from the position of the band-edge exciton and the calibration curve provided in ref 58.

Layer-by-Layer Dip Coating. To ensure a good adherence of the QDs to the quartz substrate, the quartz plate was silanized with (3-aminopropyl)triethoxysilane (APTES) in air.[59] The substrate was sonicated in a 2% Triton solution for 10 min and in ultrapure water for 5 min. Subsequently it was immersed in a 1:1 methanol/HCl solution for 30 min. Finally the substrate was silanized in a 5% APTES/ethanol solution for 1 h and rinsed with 1 mM acetic acid solution . The PbSe QD films were produced by a mechanical dip coater (DC Multi-8, Nima Technology) mounted inside a nitrogen-purged glovebox. The silanized quartz substrate was dipped alternately into a solution of PbSe QDs in hexane (~15 mM) for 60 s, a 0.1 M solution of exchanging ligands in methanol for 60 s, and a rinsing solution of methanol for 30 s. The dipping procedure was repeated 15 times, resulting in typical film thicknesses of 30−40 nm and a surface roughness of 5 nm, as determined with a Veeco Dektak 8 step-profilometer.

Optical Characterization. Optical absorption spectra were recorded with a Perkin-Elmer Lambda 900 spectrometer equipped with an integrating sphere. The spectra were corrected for scattering and reflection by first placing the film at the entrance of the integrating sphere to obtain the transmittance, F_t. Subsequently the film was placed behind the integrating sphere to obtain the reflectance, F_r; the absorptance was obtained as $F_a = 1 - F_r - F_t$ and the absorbance as $A = -\log(F_t/(1 - F_r))$.

SEM and TEM Characterization. Scanning electron microscopy was performed on QD solids deposited on indium-doped tin oxide substrates using the layer-by-layer procedure. Images were obtained with a JEOL JSM-7500F field emission SEM in secondary electron image mode at 5 kV. HR-TEM images were acquired with an aberration-corrected cubed Titan microscope operating at 300 kV. In this case PbSe QD solids were deposited onto 15 nm thick SiN membranes. To produce films that are sufficiently thin for TEM analysis only a single cycle of the LbL procedure was used.

Time-Resolved Microwave Conductivity. The photoconductance of QD solids was investigated using the time-resolved microwave conductivity technique. The samples were mounted in an X-band microwave cavity (8.4 GHz) at the position of maximum electric field (100 V/cm) for determining carrier mobilities and in an open cell without a cavity for determining carrier lifetimes. The temperature of the cavity was varied between 90 and 350 K using liquid nitrogen and power resistors. Photoexcitation laser pulses of 3 ns duration were obtained by pumping an optical parametric oscillator with the third harmonic of a Q-switched Nd:YAG laser (Opotek Vibrant 355 II). The sample was excited at 700 nm. The photon fluence I_0 was varied between 10^{11} and 10^{15} photons/cm^2/pulse, using neutral density filters. Upon photoexcitation the change in microwave power reflected was measured. For small photoinduced changes in the real conductance of the sample, $\Delta G(t)$, and negligible change in imaginary conductance, the relative change in microwave power is

$$\frac{\Delta P(t)}{P} = -K\Delta G(t) \quad (1)$$

K is a sensitivity factor that has been determined previously.[38] The photoconductance, $\Delta G(t)$, can be expressed as

$$\Delta G(t) = e\beta I_0 F_a \phi(t) \sum\mu \quad (2)$$

where e is the elementary charge, β is the ratio between the broad and narrow inner dimensions of the waveguide, I_0 is the photon fluence in the laser pulse, F_a is the fraction of light absorbed by the sample, $\phi(t)$ is the number of mobile charge carriers at time t per absorbed photon, and $\sum\mu$ is the sum of the electron and hole mobilities.

Conflict of Interest: The authors declare no competing financial interest.

Acknowledgment. The authors thank Iwan Moreels and Zeger Hens for fruitful discussions. A.J.H. acknowledges financial support from the Dutch Science Organization (NWO) through a VENI grant. This work has been financially supported by Toyota Motor Europe NV/SA and the 3TU Centre for

Sustainable Energy Technologies (Federation of the Three Universities of Technology in The Netherlands). M.A. acknowledges financial support by the Advanced Dutch Energy Materials program of the Dutch Ministry of Economic Affairs, Agriculture and Innovation.

Supporting Information Available: Additional TRMC data, FTIR spectra, additional absorption measurements, and SEM images. This material is available free of charge *via* the Internet at http://pubs.acs.org.

REFERENCES AND NOTES

1. Konstantatos, G.; Howard, I.; Fischer, A.; Hoogland, S.; Clifford, J.; Klem, E.; Levina, L.; Sargent, E. H. Ultrasensitive Solution-Cast Quantum Dot Photodetectors. *Nature* **2006**, *442*, 180–183.
2. Lee, J.-S.; Kovalenko, M. V.; Huang, J.; Chung, D. S.; Talapin, D. V. Band-Like Transport, High Electron Mobility and High Photoconductivity in All-Inorganic Nanocrystal Arrays. *Nat. Nanotechnol.* **2011**, *6*, 348–352.
3. Talapin, D. V.; Murray, C. B. PbSe Nanocrystal Solids for N- and P-Channel Thin Film Field-Effect Transistors. *Science* **2005**, *310*, 86–89.
4. Choi, J.-H.; Fafarman, A. T.; Oh, S. J.; Ko, D.-K.; Kim, D. K.; Diroll, B. T.; Muramoto, S.; Gillen, J. G.; Murray, C. B.; Kagan, C. R. Bandlike Transport in Strongly Coupled and Doped Quantum Dot Solids: A Route to High-Performance Thin-Film Electronics. *Nano Lett.* **2012**, *12*, 2631–2638.
5. Leschkies, K. S.; Beatty, T. J.; Kang, M. S.; Norris, D. J.; Aydil, E. S. Solar Cells Based on Junctions between Colloidal PbSe Nanocrystals and Thin ZnO Films. *ACS Nano* **2009**, *3*, 3638–3648.
6. Choi, J. J.; Lim, Y. F.; Santiago-Berrios, M. B.; Oh, M.; Hyun, B. R.; Sung, L. F.; Bartnik, A. C.; Goedhart, A.; Malliaras, G. G.; Abruna, H. D.; *et al*. PbSe Nanocrystal Excitonic Solar Cells. *Nano Lett.* **2009**, *9*, 3749–3755.
7. Gur, I.; Fromer, N. A.; Geier, M. L.; Alivisatos, A. P. Air-Stable All-Inorganic Nanocrystal Solar Cells Processed from Solution. *Science* **2005**, *310*, 462–465.
8. Kim, S. J.; Kim, W. J.; Cartwright, A. N.; Prasad, P. N. Carrier Multiplication in a PbSe Nanocrystal and P3HT/PCBM Tandem Cell. *Appl. Phys. Lett.* **2008**, *92*, 191107.
9. Luther, J. M.; Gao, J.; Lloyd, M. T.; Semonin, O. E.; Beard, M. C.; Nozik, A. J. Stability Assessment on a 3% Bilayer PbS/ZnO Quantum Dot Heterojunction Solar Cell. *Adv. Mater.* **2010**, *22*, 3704–3707.
10. Luther, J. M.; Law, M.; Beard, M. C.; Song, Q.; Reese, M. O.; Ellingson, R. J.; Nozik, A. J. Schottky Solar Cells Based on Colloidal Nanocrystal Films. *Nano Lett.* **2008**, *8*, 3488–3492.
11. Ma, W.; Luther, J. M.; Zheng, H. M.; Wu, Y.; Alivisatos, A. P. Photovoltaic Devices Employing Ternary PbS_xSe_{1-x} Nanocrystals. *Nano Lett.* **2009**, *9*, 1699–1703.
12. Chan, E. M.; Xu, C.; Mao, A. W.; Han, G.; Owen, J. S.; Cohen, B. E.; Milliron, D. J. Reproducible, High-Throughput Synthesis of Colloidal Nanocrystals for Optimization in Multidimensional Parameter Space. *Nano Lett.* **2010**, *10*, 1874–1885.
13. Kovalenko, M. V.; Talapin, D. V.; Loi, M. A.; Cordella, F.; Hesser, G.; Bodnarchuk, M. I.; Heiss, W. Quasi-Seeded Growth of Ligand-Tailored PbSe Nanocrystals through Cation-Exchange-Mediated Nucleation. *Angew. Chem., Int. Ed.* **2008**, *47*, 3029–3033.
14. Moreels, I.; Justo, Y.; De Geyter, B.; Haustraete, K.; Martins, J. C.; Hens, Z. Size-Tunable, Bright, and Stable PbS Quantum Dots: A Surface Chemistry Study. *ACS Nano* **2011**, *5*, 2004–2012.
15. Guyot-Sionnest, P.; Wang, C. Fast Voltammetric and Electrochromic Response of Semiconductor Nanocrystal Thin Films. *J. Phys. Chem. B* **2003**, *107*, 7355–7359.
16. Kovalenko, M. V.; Scheele, M.; Talapin, D. V. Colloidal Nanocrystals with Molecular Metal Chalcogenide Surface Ligands. *Science* **2009**, *324*, 1417–1420.
17. Fafarman, A. T.; Koh, W. K.; Diroll, B. T.; Kim, D. K.; Ko, D. K.; Oh, S. J.; Ye, X. C.; Doan-Nguyen, V.; Crump, M. R.; Reifsnyder, D. C.; *et al*. Thiocyanate-Capped Nanocrystal Colloids: Vibrational Reporter of Surface Chemistry and Solution-Based Route to Enhanced Coupling in Nanocrystal Solids. *J. Am. Chem. Soc.* **2011**, *133*, 15753–15761.
18. Nag, A.; Kovalenko, M. V.; Lee, J. S.; Liu, W. Y.; Spokoyny, B.; Talapin, D. V. Metal-Free Inorganic Ligands for Colloidal Nanocrystals: S^{2-}, HS^-, Se^{2-}, HSe^-, Te^{2-}, HTe^-, TeS_3^{2-}, OH^-, and NH_2^- as Surface Ligands. *J. Am. Chem. Soc.* **2011**, *133*, 10612–10620.
19. Tang, J.; Kemp, K. W.; Hoogland, S.; Jeong, K. S.; Liu, H.; Levina, L.; Furukawa, M.; Wang, X.; Debnath, R.; Cha, D.; *et al*. Colloidal-Quantum-Dot Photovoltaics Using Atomic-Ligand Passivation. *Nat. Mater.* **2011**, *10*, 765–771.
20. Talgorn, E. T; Abellon, R. D.; Savenije, T. J.; Goossens, A.; Houtepen, A. J.; Siebbeles, L. D. A. Highly Photoconductive CdSe Quantum-Dot Films: Influence of Capping Molecules and Film Preparation Procedure. *J. Phys. Chem. C* **2010**, *114*, 3441–3447.
21. Luther, J. M.; Law, M.; Song, Q.; Perkins, C. L.; Beard, M. C.; Nozik, A. J. Structural, Optical and Electrical Properties of Self-Assembled Films of PbSe Nanocrystals Treated with 1,2-Ethanedithiol. *ACS Nano* **2008**, *2*, 271–280.
22. Law, M.; Luther, J. M.; Song, O.; Hughes, B. K.; Perkins, C. L.; Nozik, A. J. Structural, Optical, and Electrical Properties of PbSe Nanocrystal Solids Treated Thermally or with Simple Amines. *J. Am. Chem. Soc.* **2008**, *130*, 5974–5985.
23. Murphy, J. E.; Beard, M. C.; Nozik, A. J. Time-Resolved Photoconductivity of PbSe Nanocrystal Arrays. *J. Phys. Chem. B* **2006**, *110*, 25455–25461.
24. Williams, K. J.; Tisdale, W. A.; Leschkies, K. S.; Haugstad, G.; Norris, D. J.; Aydil, E. S.; Zhu, X. Y. Strong Electronic Coupling in Two-Dimensional Assemblies of Colloidal PbSe Quantum Dots. *ACS Nano* **2009**, *3*, 1532–1538.
25. Sarasqueta, G.; Choudhury, K. R.; So, F. Effect of Solvent Treatment on Solution-Processed Colloidal PbSe Nanocrystal Infrared Photodetectors. *Chem. Mater.* **2010**, *22*, 3496–3501.
26. Law, M.; Beard, M. C.; Choi, S.; Luther, J. M.; Hanna, M. C.; Nozik, A. J. Determining the Internal Quantum Efficiency of PbSe Nanocrystal Solar Cells with the Aid of an Optical Model. *Nano Lett.* **2008**, *8*, 3904–3910.
27. Tang, J.; Brzozowski, L.; Barkhouse, D. A. R.; Wang, X. H.; Debnath, R.; Wolowiec, R.; Palmiano, E.; Levina, L.; Pattantyus-Abraham, A. G.; Jamakosmanovic, D.; *et al*. Quantum Dot Photovoltaics in the Extreme Quantum Confinement Regime: The Surface-Chemical Origins of Exceptional Air- and Light-Stability. *ACS Nano* **2010**, *4*, 869–878.
28. Liu, Y.; Gibbs, M.; Puthussery, J.; Gaik, S.; Ihly, R.; Hillhouse, H. W.; Law, M. Dependence of Carrier Mobility on Nanocrystal Size and Ligand Length in PbSe Nanocrystal Solids. *Nano Lett.* **2010**, *10*, 1960–1969.
29. Koleilat, G. I.; Levina, L.; Shukla, H.; Myrskog, S. H.; Hinds, S.; Pattantyus-Abraham, A. G.; Sargent, E. H. Efficient, Stable Infrared Photovoltaics Based on Solution-Cast Colloidal Quantum Dots. *ACS Nano* **2008**, *2*, 833–840.
30. Barkhouse, D. A. R.; Pattantyus-Abraham, A. G.; Levina, L.; Sargent, E. H. Thiols Passivate Recombination Centers in Colloidal Quantum Dots Leading to Enhanced Photovoltaic Device Efficiency. *ACS Nano* **2008**, *2*, 2356–2362.
31. Zhao, N.; Osedach, T. P.; Chang, L.-Y.; Geyer, S. M.; Wanger, D.; Binda, M. T.; Arango, A. C.; Bawendi, M. G.; Bulovic, V. Colloidal PbS Quantum Dot Solar Cells with High Fill Factor. *ACS Nano* **2010**, *4*, 3743–3752.
32. Choi, J. J.; Luria, J.; Hyun, B. R.; Bartnik, A. C.; Sun, L. F.; Lim, Y. F.; Marohn, J. A.; Wise, F. W.; Hanrath, T. Photogenerated Exciton Dissociation in Highly Coupled Lead Salt Nanocrystal Assemblies. *Nano Lett.* **2010**, *10*, 1805–1811.
33. Zarghami, M. H.; Liu, Y.; Gibbs, M.; Gebremichael, E.; Webster, C.; Law, M. P-Type PbSe and PbS Quantum Dot Solids Prepared with Short-Chain Acids and Diacids. *ACS Nano* **2010**, *4*, 2475–2485.
34. Gao, Y.; Talgorn, E.; Aerts, M.; Trinh, M. T.; Schins, J. M.; Houtepen, A. J.; Siebbeles, L. D. A. Enhanced Hot-Carrier Cooling and Ultrafast Spectral Diffusion in Strongly Coupled PbSe Quantum-Dot Solids. *Nano Lett.* **2011**, *11*, 5471–5476.

35. Wolcott, A.; Doyeux, V.; Nelson, C. A.; Gearba, R.; Lei, K. W.; Yager, K. G.; Dolocan, A. D.; Williams, K.; Nguyen, D.; Zhu, X. Y. Anomalously Large Polarization Effect Responsible for Excitonic Red Shifts in PbSe Quantum Dot Solids. *J. Phys. Chem. Lett.* **2011**, *2*, 795–800.
36. Guyot-Sionnest, P. Electrical Transport in Colloidal Quantum Dot Films. *J. Phys. Chem. Lett.* **2012**, *3*, 1169–1175.
37. Talgorn, E.; Abellon, R. D.; Kooyman, P. J.; Piris, J.; Savenije, T. J.; Goossens, A.; Houtepen, A. J.; Siebbeles, L. D. A. Supercrystals of CdSe Quantum Dots with High Charge Mobility and Efficient Electron Transfer to TiO_2. *ACS Nano* **2010**, *4*, 1723–1731.
38. Savenije, T. J.; de Haas, M. P.; Warman, J. M. The Yield and Mobility of Charge Carriers in Smooth and Nanoporous TiO_2 Films. *Z. Phys. Chem.* **1999**, *212*, 201–206.
39. Talgorn, E.; de Vries, M. A.; Siebbeles, L. D. A.; Houtepen, A. J. Photoconductivity Enhancement in Multilayers of CdSe and CdTe Quantum Dots. *ACS Nano* **2011**, *5*, 3552–3558.
40. Moreels, I.; Lambert, K.; De Muynck, D.; Vanhaecke, F.; Poelman, D.; Martins, J. C.; Allan, G.; Hens, Z. Composition and Size-Dependent Extinction Coefficient of Colloidal PbSe Quantum Dots. *Chem. Mater.* **2007**, *19*, 6101–6106.
41. Talgorn, E.; Gao, Y.; Aerts, M.; Kunneman, L. T.; Schins, J. M.; Savenije, T. J.; van Huis, M. A.; van der Zant, H. S. J.; Houtepen, A. J.; Siebbeles, L. D. A. Unity Quantum Yield of Photogenerated Charges and Band-Like Transport in Quantum-Dot Solids. *Nat. Nanotechnol.* **2011**, *6*, 733–739.
42. Fritzinger, B.; Moreels, I.; Lommens, P.; Koole, R.; Hens, Z.; Martins, J. C. *In Situ* Observation of Rapid Ligand Exchange in Colloidal Nanocrystal Suspensions Using Transfer NOE Nuclear Magnetic Resonance Spectroscopy. *J. Am. Chem. Soc.* **2009**, *131*, 3024–3032.
43. Ojha, A. K.; Chandra, G.; Roy, A. A Study on Adsorption of Acetonitrile on Gold Nanorods by Non-Resonant Raman Measurements and Density Functional Theory Calculations. *Nanotechnology* **2008**, *19*, 095706.
44. Solomun, T.; Christmann, K.; Baumgaertel, H. Interaction of Acetonitrile and Benzonitrile with the Gold (100) Surface. *J. Phys. Chem.* **1989**, *93*, 7199–7208.
45. Strange, M.; Rostgaard, C.; H√§kkinen, H.; Thygesen, K. S. Self-Consistent Gw Calculations of Electronic Transport in Thiol- and Amine-Linked Molecular Junctions. *Phys. Rev. B* **2011**, *83*, 115108.
46. Kiguchi, M.; Nakamura, H.; Takahashi, Y.; Takahashi, T.; Ohto, T. Effect of Anchoring Group Position on Formation and Conductance of a Single Disubstituted Benzene Molecule Bridging Au Electrodes: Change of Conductive Molecular Orbital and Electron Pathway. *J. Phys. Chem. C* **2010**, *114*, 22254–22261.
47. Chen, F.; Li, X.; Hihath, J.; Huang, Z.; Tao, N. Effect of Anchoring Groups on Single-Molecule Conductance: A Comparative Study of Thiol-, Amine-, and Carboxylic-Acid-Terminated Molecules. *J. Am. Chem. Soc.* **2006**, *128*, 15874–15881.
48. Kim, Y.; Hellmuth, T. J.; Burkle, M.; Pauly, F.; Scheer, E. Characteristics of Amine-Ended and Thiol-Ended Alkane Single-Molecule Junctions Revealed by Inelastic Electron Tunneling Spectroscopy. *ACS Nano* **2011**, *5*, 4104–4111.
49. Koole, R.; Luigjes, B.; Tachiya, M.; Pool, R.; Vlugt, T. J. H.; Donega, C. D. M.; Meijerink, A.; Vanmaekelbergh, D. Differences in Cross-Link Chemistry between Rigid and Flexible Dithiol Molecules Revealed by Optical Studies of CdTe Quantum Dots. *J. Phys. Chem. C* **2007**, *111*, 11208–11215.
50. Miller, A.; Abrahams, E. Impurity Conduction at Low Concentrations. *Phys. Rev.* **1960**, *120*, 745–755.
51. Houtepen, A. J.; Kockmann, D.; Vanmaekelbergh, D. Reappraisal of Variable-Range Hopping in Quantum-Dot Solids. *Nano Lett.* **2008**, *8*, 3516–3520.
52. In ref 28 the reported value of the tunneling decay constant is 1.1 Å based on the relation $\mu = \mu_0 \exp(-0.865\beta)$. The factor 0.865 in the exponent is the result of percolation theory. As it is not clear to us to what extent this percolation theory applies to the systems investigated here, we did not take it into account.
53. Salomon, A.; Cahen, D.; Lindsay, S.; Tomfohr, J.; Engelkes, V. B.; Frisbie, C. D. Comparison of Electronic Transport Measurements on Organic Molecules. *Adv. Mater.* **2003**, *15*, 1881–1890.
54. Wehrenberg, B. L.; Wang, C. J.; Guyot-Sionnest, P. Interband and Intraband Optical Studies of PbSe Colloidal Quantum Dots. *J. Phys. Chem. B* **2002**, *106*, 10634–10640.
55. Luther, J. Private communication.
56. Semonin, O. E.; Luther, J. M.; Choi, S.; Chen, H.-Y.; Gao, J.; Nozik, A. J.; Beard, M. C. Peak External Photocurrent Quantum Efficiency Exceeding 100% *via* MEG in a Quantum Dot Solar Cell. *Science* **2011**, *334*, 1530–1533.
57. Szendrei, K.; Gomulya, W.; Yarema, M.; Heiss, W.; Loi, M. A. PbS Nanocrystal Solar Cells with High Efficiency and Fill Factor. *Appl. Phys. Lett.* **2010**, 97.
58. Koole, R.; Allan, G.; Delerue, C.; Meijerink, A.; Vanmaekelbergh, D.; Houtepen, A. J. Optical Investigation of Quantum Confinement in PbSe Nanocrystals at Different Points in the Brillouin Zone. *Small* **2008**, *4*, 127–133.
59. Han, Y.; Mayer, D.; Offenhausser, A.; Ingebrandt, S. Surface Activation of Thin Silicon Oxides by Wet Cleaning and Silanization. *Thin Solid Films* **2006**, *510*, 175–180.